

PSFC/JA-08-31

**Observation of Ion Cyclotron Range of Frequencies
Mode Conversion Flow Drive in Tokamak Plasmas***

Lin, Y., Rice, J.E., Wukitch, S. J., Greenwald, M.J.,
Hubbard, A.E., Ince-Cushman, A., Lin, L.,
Porkolab, M., Reinke, M., and Tsujii, N

October 2008

**Plasma Science and Fusion Center
Massachusetts Institute of Technology
Cambridge MA 02139 USA**

This work was supported by the U.S. Department of Energy, Cooperative agreement No. DE-FC02-99ER54512. Reproduction, translation, publication, use and disposal, in whole or in part, by or for the United States government is permitted.

* To be published on Phys. Rev. Lett.

Observation of Ion Cyclotron Range of Frequencies Mode Conversion Flow Drive in Tokamak Plasmas

Y. Lin,* J.E. Rice, S.J. Wukitch, M.J. Greenwald, A.E. Hubbard,
A. Ince-Cushman, L. Lin, M. Porkolab, M.L. Reinke, and N. Tsujii

Massachusetts Institute of Technology,

Plasma Science and Fusion Center, Cambridge, MA 02139, USA

(Dated: October 28, 2008)

Abstract

Strong toroidal flow (V_ϕ) and poloidal flow (V_θ) have been observed in D-³He plasmas with ion cyclotron range of frequencies (ICRF) mode conversion (MC) heating on the Alcator C-Mod tokamak. The toroidal flow scales with the rf power P_{rf} (up to 30 km/s per MW), and is significantly larger than that in ICRF minority heated plasmas at the same rf power or stored energy. The central V_ϕ responds to P_{rf} faster than the outer regions, and the $V_\phi(r)$ profile is broadly peaked for $r/a \leq 0.5$. Localized ($0.3 \leq r/a \leq 0.5$) V_θ appears when $P_{rf} \geq 1.5$ MW and increases with power (up to 0.7 km/s per MW). The experimental evidence together with numerical wave modeling suggests a local flow drive source due to the interaction between the MC ion cyclotron wave and ³He ions.

PACS numbers: 52.55.Fa, 52.50.Qt, 52.35.Hr, 52.30.-q

Plasma flow and velocity shear can be important in stabilizing micro- and macro-instabilities (like drift wave turbulence [1, 2] or resistive wall modes [3]) in tokamak plasmas. For ITER and even more so for reactors, the input torque from neutral beam injection will be low or non-existent, and beam penetration and accompanying deposition profile control are limited. Plasma intrinsic rotation (spontaneous, without momentum input) may be sufficient for resistive wall mode stabilization on ITER [4], but it does not allow simple external control. Externally launched electromagnetic radio frequency (rf) waves may offer the possibility of controlled rotation drive on ITER and reactors. RF poloidal flow drive may also offer a unique means for manipulating transport via flow shear stabilization in reactor relevant regimes - thus affecting pressure profiles, bootstrap current, etc. As a result, rf flow drive has been widely identified as a high leverage tool that, if successful, can produce great benefits to tokamak research.

Ion cyclotron range of frequencies (ICRF) waves have been utilized to drive plasma flow. Kinetic Alfvén waves were observed to drive plasma flow on the Phaedrus-T tokamak [5]. Poloidal flow driven by direct launch ion Bernstein waves (IBW) was detected on Tokamak Fusion Test Reactor (TFTR) [6]. Using directed fast magnetosonic wave (fast wave, or FW), toroidal rotation was observed to be driven by wave momentum absorption by fast ions on the JET tokamak [7]. Preliminary evidence of poloidal flow drive was observed on TFTR through mode conversion (MC) [8]. Here we report the first demonstration of efficient toroidal flow (V_ϕ) drive and also observation of poloidal flow (V_θ) generation via the ICRF MC process. The experimental evidence together with numerical wave modeling suggests a local flow drive source due to the interaction between the MC ion cyclotron wave (ICW) and ^3He ions.

On the Alcator C-Mod tokamak ($R = 0.67$ m and $a = 0.22$ m), fast waves at 80 MHz and 50 MHz are launched externally from the low field side (LFS), either separately or combined [9]. For the results reported here, plasma current $I_p \simeq 0.8$ MA, and magnetic field $B_{t0} \simeq 5.1$ T. The 80 MHz fast wave heats the plasma via D(H) minority heating (MH) with residual $n_H/n_e \leq 5\%$. The fast wave power is first deposited to the minority H ions via ion cyclotron (IC) resonance, $R_{IC,H} \simeq 0.65$ m, slightly on the high field side (HFS) of the magnetic axis, and then the energetic H ions transfer their energy to the bulk electrons and majority deuterium ions when they slow down through collisions. In D- ^3He plasma with moderate ^3He concentration (e.g., $n_{^3\text{He}}/n_e \geq 5\%$), the 50 MHz fast wave ($R_{IC,^3\text{He}} \simeq 0.71$

m) can be mostly converted to short wavelength slow waves, ICW and IBW, near the MC surface (also called D-³He hybrid layer), and directly heat electrons and ions [10–14].

For the first time in tokamaks, we have observed significant toroidal flow driven by the ICRF MC process. In Fig. 1, we compare the central rotation velocity $V_\phi(r = 0)$ of two upper-single-null plasmas in low confinement mode (L-mode) with the same electron density but with different ICRF applications: one using the 80 MHz wave in dipole phase (MH), and the other using the 50 MHz wave (MC) phased at $+90^\circ$ (i.e., wave traveling in the co-current direction). The toroidal flow (rotation) velocity, derived from the Doppler shift of the x-ray spectra of Ar¹⁷⁺ impurity measured by high resolution x-ray spectroscopy (HIREX) [15], is significantly higher in the MC plasma than that in the MH plasma as shown Fig. 1-(a). In the MC plasma, $V_\phi(r = 0)$ rises from -10 km/sec (counter-current direction), a typical value in ohmic L-mode plasma, to $+75$ km/sec (110 kRad/s, and $M_A = V_\phi/C_A \sim 0.013$, where M_A is the Alfvén Mach number and C_A is the Alfvén velocity) in the co-current direction with 3 MW rf power. The velocity change ΔV_ϕ is approximately linear vs. P_{rf} , indicating a mechanism in which the rf power dissipation is important, rather than a mechanism directly related to the rf field strength. In contrast, in the MH plasma at approximately the same P_{rf} and heating history as the MC plasma, $V_\phi(r = 0)$ only rises to $+20$ km/sec. Strong co-current rotation has been observed in many MC plasmas where $5.0 \leq B_t \leq 5.2$ T and both IC resonance and MC surface are near-axis. The rotation is largely independent of antenna phase. While the magnitude at $+90^\circ$ phase is larger than those in dipole and -90° phases, the difference is fairly small ($< 10\%$). When compared with the empirically determined intrinsic rotation scaling law $\Delta V_\phi \propto \Delta W_p/I_p$ [16–18], the rotation change in these MC plasmas is generally a factor ≥ 2 larger than that from MH plasmas with identical plasma shape, magnetic field, current and density.

Unlike the intrinsic toroidal rotation, which propagates inward from the edge through momentum pinch and diffusion [19, 20], the toroidal rotation in MC plasmas rises first near the plasma center. In Fig. 2 we compare the time traces of ΔV_ϕ at $r/a \simeq 0, 0.3$ and 0.7 of an MC plasma. Both velocities at $r/a = 0$ and 0.3 rise to a steady value in less than 80 ms after the application of the 50 MHz rf power, while $\Delta V_\phi(r/a \simeq 0.7)$ is delayed and with a much smaller magnitude. The difference in the response to rf power also creates a broad centrally peaked $V_\phi(r/a)$ profile in MC plasmas. In Fig. 3-(a), we compare the chord integrated rotation profiles obtained from Ar¹⁶⁺ of the two plasmas in Fig. 1. $V_\phi(r/a)$

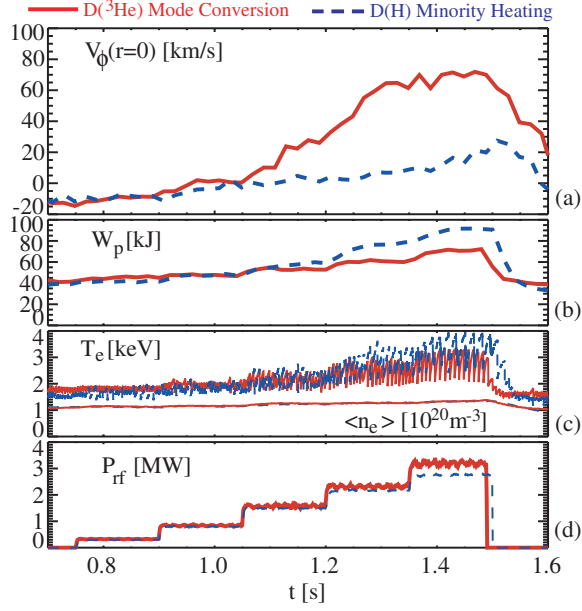


FIG. 1: (color online). (a) Change of plasma central rotation $V_\phi(r=0)$ after the application of rf power at 0.75 sec in an MC plasma (red solid lines) and an MH plasma (blue dashed lines). Plasma stored energy W_p , T_e , $\langle n_e \rangle$, and P_{rf} are shown in (b), (c), and (d).

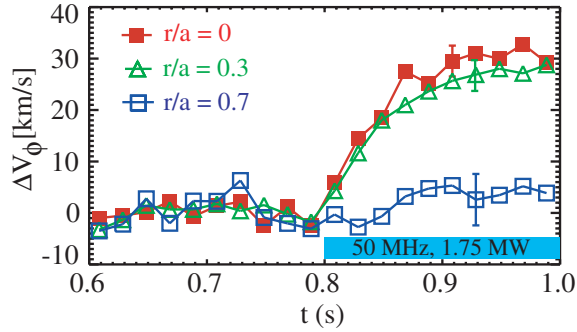


FIG. 2: (color online). V_ϕ traces at different r/a . The traces have been shifted to have $\langle V_\phi \rangle \simeq 0$ for $t < 0.8$ sec.

profiles before the rf application at $t = 0.7$ s are both flat. When heated with the rf power at $t = 1.4$ s, the rotation profile in the MH plasma is slightly hollow, typical in L-mode plasmas [19, 20]. In contrast, $V_\phi(r/a)$ of the MC plasma is broadly peaked within $r/a \leq 0.5$, but at a similar level to that of the MH plasma in the outer region ($r/a \geq 0.5$). In Fig. 3-(b), the Ar^{16+} ion temperature profiles show that the MC plasma has a higher T_i than that of the MH plasma for $r/a \leq 0.5$, while it has a somewhat lower T_e as seen in Fig. 1-(c).

Concomitant to the strong toroidal rotation, a poloidal flow V_θ in the ion diamagnetic

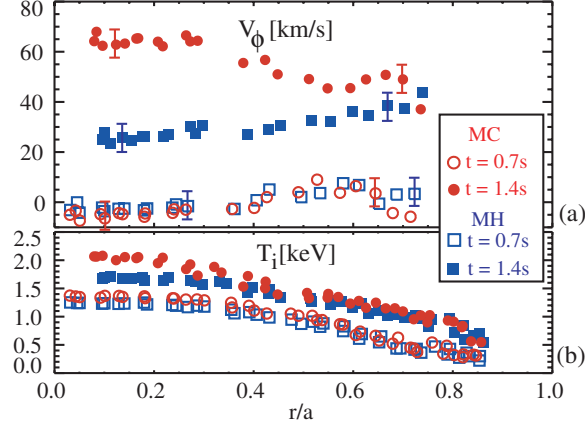


FIG. 3: (color online). (a) Chord integrated V_ϕ profile (systematic error are about ± 10 km/s), and (b) T_i (Ar^{16+}) profile of the MC and MH plasmas in Fig. 1 at two time points.

direction is observed in the MC plasma. Since HIREX measures a combination of toroidal and poloidal components, V_θ is derived from the difference of the velocities measured by two chords viewing symmetrically above and below the mid-plane and tangential to a flux surface to remove the toroidal component. In Fig. 4-(a), $\Delta V_\theta(r/a)$ at different rf power levels in the MC and MH plasmas are compared. In the MH plasma, there is no detectable poloidal flow, while in the MC plasma, a significant flow appears in the region of $0.3 \leq r/a \leq 0.5$, and peaks at ~ 0.7 km/s per MW rf power. In Fig. 5-(b), the peak poloidal velocity $\Delta V_\theta(r/a = 0.44)$ is plotted vs. time, and it shows that the flow becomes significant when $P_{rf} \geq 1.5$ MW and increases with P_{rf} (Fig. 5-(c)). Interestingly, the density fluctuation spectra, measured by a phase contrast imaging (PCI) system [10], show a turbulence frequency broadening following the same trend as V_θ (Fig. 5-(a)), indicating a change in bulk ions flow as well.

MC waves are detected by the vertical chords of PCI in the region of $-4 \leq R - R_{axis} \leq -2$ cm. The wavenumber k_R of the MC waves is $\sim 4 - 5$ cm^{-1} , close to previous results in D- ^3He plasmas at similar field and rf frequency [13]. During the MC process, part of the mode converted power heats the electrons directly through electron Landau damping (ELD). Fig. 6-(a) shows the direct electron heating profile, derived from the break-in-slope of T_e traces at $t = 1.49$ s (fast rf shutoff), $P_e \simeq \frac{3}{2} n_e \Delta(\frac{dT_e}{dt})$ [12], of the MC plasma from two independent electron cyclotron emission (ECE) T_e diagnostics. The integrated power to electrons is estimated to be ~ 0.42 MW out of the total 3 MW input rf power.

The two-dimensional (2-D) full-wave code TORIC [21] has been used to simulate the MC

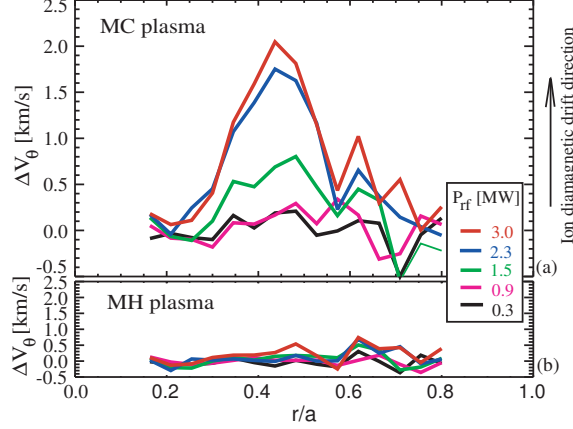


FIG. 4: (color online). Poloidal rotation velocity in (a) MC plasma and (b) MH plasma. V_θ before the rf application is subtracted. Uncertainties are approximately ± 0.5 km/s.

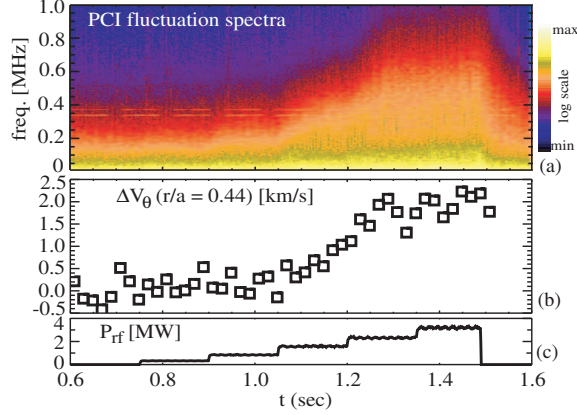


FIG. 5: (color online). (a) PCI turbulence power spectra in frequency and time, (b) Poloidal rotation vs time, and (c) P_{rf} vs. time.

plasma. In Fig. 6-(b), we plot power deposition profiles obtained from TORIC runs, weighted summing over the entire antenna toroidal mode (n_ϕ) spectrum of 90° phase ($+1 \leq n_\phi \leq +12$). The species mix in the simulation is iteratively determined to be $n_{3He}/n_e \simeq 8 - 10\%$ so that the peak electron deposition matches that in Fig. 6-(a). The location of the MC wave field also matches that from the PCI wave measurement. The total electron deposition from the simulation is 0.6 MW out of 3 MW, and 2.2 MW of the power is absorbed by the ^3He ions, with the rest 0.2 MW to D ions. The ^3He deposition profile shown in Fig. 6-(b) is broadly peaked within $r/a \leq 0.5$, but decreases in the outer region.

From the TORIC simulation, we find the power deposition to the ^3He ions is mostly

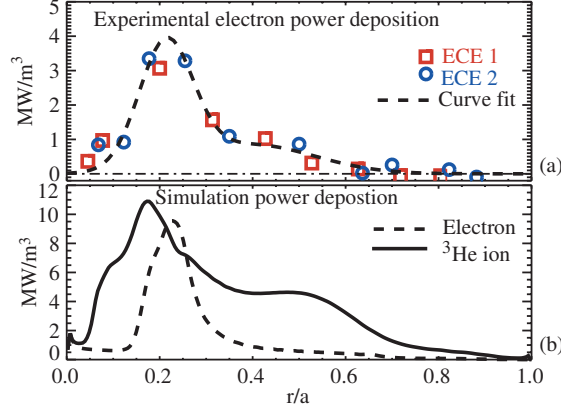


FIG. 6: (color online). (a) Direct electron heating power deposition profile from ECE; (b) Power deposition to electrons and ^3He ions from TORIC simulation.

through the MC ICW, rather than through the fast wave as in MH plasmas. In Fig. 7, we show the 2-D power deposition profiles from the TORIC run with $n_\phi = +6$. In Fig. 7-(a), the ion deposition by the MC ICW is shown to be more than an order of magnitude larger than that by the FW. Fig. 7-(b) shows a weak electron deposition by the MC ICW but strong electron heating by the MC IBW on the HFS of the MC layer. The MC ICW deposition is within several cm on the LFS of the MC layer, and strongest at $\sim 7 - 12$ cm vertically below and above the mid-plane, where a larger poloidal B field makes the mode conversion to ICW possible [13, 14]. These peak deposition regions map to the flux surfaces of $0.3 < r/a < 0.5$, the same location where local poloidal flow is observed (Fig. 4-(a)). Numerically solving the full electromagnetic wave dispersion equation finds that the ICW k_{\parallel} is up-shifted from the FW level of 10 m^{-1} to $k_{\parallel} \sim 40 - 50 \text{ m}^{-1}$ [10, 14], and the IC resonance condition $\omega \simeq \Omega_{c,^3\text{He}} + k_{\parallel}v_{t,^3\text{He}}$ can be satisfied in the vicinity of the MC surface, about 4 cm away on the HFS of the IC resonance. This is consistent with the TORIC simulation showing that significant ion damping of the ICW occurs near the MC surface.

The involvement of slow wave and resonant wave-ion interaction is consistent with previous theoretical work on rf flow drive [14, 22–24]. Analytical estimates for V_ϕ and V_θ generated by direct-launch IBW at the diffusive limit were presented in Eqs. (45) and (43) in Ref. [23],

$$V_\phi [km/s] \sim \frac{48P_{rf}[MW]k_{\parallel}[m^{-1}]}{R[m]f[MHz]D[m^2/s]n_{20}\mu} \quad (1)$$

$$V_\theta [km/s] \sim \frac{0.4P_{rf}[MW]}{q^2R[m]r[m]B[T]D[m^2/s]n_{20}}. \quad (2)$$

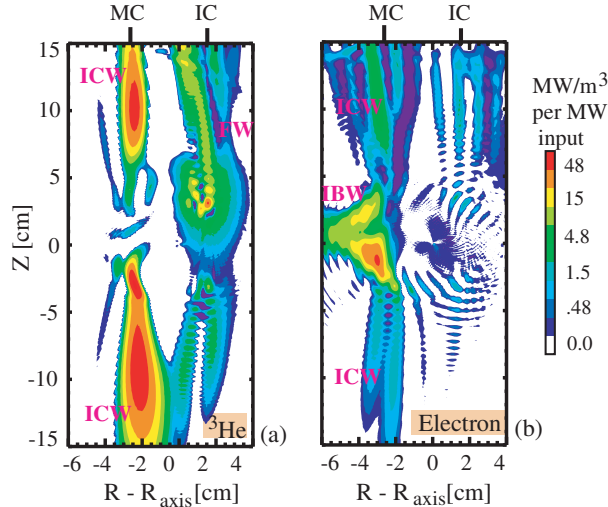


FIG. 7: (color online). 2-D power deposition from TORIC simulation: (a) Power to ^3He , (b) Power to electrons. The MC surface and ^3He IC resonance are also labeled.

Using the parameters of the MC plasma in Fig. 1, $B \simeq 5.1$ T, $n_{20} \simeq 1.3$, $R \simeq 0.7$ m, $r \simeq 0.1$ m, $k_{\parallel} \simeq 40$ m $^{-1}$, $f = 50$ MHz, local $q \simeq 1.6$ and effective $\mu = \sum n_i m_i / \sum n_i m_p \simeq 2.1$ [25], and L-mode momentum diffusion coefficient $D \simeq 0.2$ m 2 /s [19, 20], we have $V_{\phi} \sim 10^2$ km/s and $V_{\theta} \sim 2$ km/s per MW. Assuming that the MC ICW (about half of the total input power) interacts with ions similarly to direct launch IBW, these estimates are comparable to our experimental observation.

On ITER and other future burning plasma devices, ICRF mode conversion can be utilized in H- ^3He plasmas during the non-radioactive phase and in D-T plasmas during the radioactive phase. By carefully selecting the rf frequency, B field, antenna phase, species mix and other plasma parameters, it may be possible to drive substantial toroidal plasma rotation and also generate significant poloidal flow.

The authors thank the Alcator C-Mod operation and ICRF groups, and E. Edlund for PCI system setup and operation. This research utilized the MIT Plasma Science and Fusion Center Theory Group parallel computational cluster. This work was supported at MIT by U.S. DoE Cooperative Agreement No. DE-FC02-99ER54512.

* Email: ylin@psfc.mit.edu

[1] G. G. Craddock and P. H. Diamond, Phys. Rev. Lett. **67**, 1535 (1991).

- [2] P. W. Terry, *Rev. Mod. Phys.* **72**, 109 (2000).
- [3] E. J. Strait, T. S. Taylor, A. D. Turnbull, et al., *Phys. Rev. Lett.* **74**, 2483 (1995).
- [4] J. E. Rice, A. Ince-Cushman, J. S. deGrassie, et al., *Nucl. Fusion* **47**, 1618 (2007).
- [5] S. J. Wukitch, C. Litwin, M. Harper, R. Parker, and N. Hershkowitz, *Phys. Rev. Lett.* **77**, 294 (1996).
- [6] B. P. LeBlanc, R. E. Bell, S. Bernabei, et al., *Phys. Rev. Lett.* **82**, 331 (1999).
- [7] L.-G. Eriksson, T. Johnson, T. Hellsten, et al., *Phys. Rev. Lett.* **92**, 235001 (2004).
- [8] C. K. Phillips, M. G. Bell, R. E. Bell, et al., *Nucl. Fusion* **40**, 461 (2000).
- [9] P. T. Bonoli, R. Parker, S. J. Wukitch, Y. Lin, M. Porkolab, et al., *Fusion Sci. Technol.* **51**, 401 (2007).
- [10] E. Nelson-Melby, M. Porkolab, P. T. Bonoli, Y. Lin, A. Mazurenko, and S. J. Wukitch, *Phys. Rev. Lett.* **90**, 155004 (2003).
- [11] Y. Lin, S. J. Wukitch, P. T. Bonoli, et al., *Phys. Plasmas* **11**, 2466 (2004).
- [12] Y. Lin, S. J. Wukitch, P. T. Bonoli, et al., *Plasma Phys. Control. Fusion* **45**, 1013 (2003).
- [13] Y. Lin, S. J. Wukitch, A. Parisot, et al., *Plasma Phys. Control. Fusion* **47**, 1207 (2005).
- [14] E. F. Jaeger, L. A. Berry, J. R. Myra, et al., *Phys. Rev. Lett.* **90**, 195001 (2003).
- [15] A. Ince-Cushman, J. E. Rice, M. Bitter, et al., *Spatially resolved high resolution x-ray spectroscopy for magnetically confined fusion plasmas*, submitted to *Rev. Sci. Instrum.*
- [16] J. E. Rice, P. T. Bonoli, J. A. Goetz, et al., *Nucl. Fusion* **39**, 1175 (1999).
- [17] J. E. Rice, R. L. Boivin, P. T. Bonoli, et al., *Nucl. Fusion* **41**, 277 (2001).
- [18] J. E. Rice, A. E. Hubbard, J. W. Hughes, et al., *Nucl. Fusion* **45**, 251 (2005).
- [19] W. D. Lee, J. E. Rice, E. S. Marmor, et al., *Phys. Rev. Lett.* **91**, 205003 (2003).
- [20] J. E. Rice, W. D. Lee, E. S. Marmor, et al., *Nucl. Fusion* **44**, 379 (2004).
- [21] J. C. Wright, P. T. Bonoli, M. Brambilla, et al., *Phys. Plasmas* **11**, 2473 (2004).
- [22] L. A. Berry, E. F. Jaeger, and D. B. Batchelor, *Phys. Rev. Lett.* **82**, 1871 (1999).
- [23] J. R. Myra and D. A. D'Ippolito, *Phys. Plasmas* **9**, 3867 (2002).
- [24] J. R. Myra, L. A. Berry, D. A. D'Ippolito, and E. F. Jaeger, *Phys. Plasmas* **11**, 1786 (2004).
- [25] J. R. Myra, private communication. The definition of μ in Ref. [22] had an error and it should be m_i/m_p .